IATSS Research 42 (2018) 248–258

Contents lists available at ScienceDirect

IATSS Research

Research article

Towards lane-level traffic monitoring in urban environment using precise probe vehicle data derived from three-dimensional map aided differential GNSS

Yanlei Gu [a,*], Li-Ta Hsu [b], Shunsuke Kamijo [a]

[a] The University of Tokyo, Japan
[b] Hong Kong Polytechnic University, China

ARTICLE INFO

Article history:
Received 29 May 2017
Received in revised form 9 March 2018
Accepted 12 March 2018
Available online 21 March 2018

Keywords:
Probe data
Differential GNSS
3D building map
Vehicle localization
Stop detection
Lane-change detection

ABSTRACT

Today's urban road transport systems experience increasing congestion that threatens the environment and transport efficiency. Global Navigation Satellite System (GNSS)-based vehicle probe technology has been proposed as an effective means for monitoring the traffic situation and can be used for future city development. More specifically, lane-level traffic analysis is expected to provide an effective solution for traffic control. However, GNSS positioning technologies suffer from multipath and Non-Line-Of-Sight (NLOS) propagations in urban environments. The multipath and NLOS propagations severely degrade the accuracy of probe vehicle data. Recently, a three-dimensional (3D) city map became available on the market. We propose to use the 3D building map and differential correction information to simulate the reflecting path of satellite signal transmission and improve the results of the commercial GNSS single-frequency receiver, technically named 3D map-aided Differential GNSS (3D-DGNSS). In this paper, the innovative 3D-DGNSS is employed for the acquisition of precise probe vehicle data. In addition, this paper also utilizes accelerometer-based lane change detection to improve the positioning accuracy of probe vehicle data. By benefitting from the proposed method, the lane-level position, vehicle speed, and stop state of vehicles were estimated. Finally, a series of experiments and evaluations were conducted on probe data collected in one of the most challenging urban cities, Tokyo. The experimental results show that the proposed method has a correct lane localization rate of 87% and achieves sub-meter accuracy with respect to the position and speed error means. The accurate positioning data provided by the 3D-DGNSS result in a correct detection rate of the stop state of vehicles of 92%.

1. Introduction

With the increase of urban populations, cities face the challenge to meet the rising demand for efficient mobility within limited infrastructure capacity. Global Navigation Satellite System (GNSS) based vehicle probe technology is emerging as an effective means for monitoring traffic flow and optimizing traffic control [1]. The vehicle position, speed, time, and other information based on probe data allow the development of transformative applications that can improve roadway operations, planning, and maintenance and keep travelers informed about travel conditions [2–5]. To suggest an effective solution, such as lane-level traffic analysis, the accuracy of vehicle localization based on probe data is expected to be sub-meter level or even more precise [6,7].

Recently, many sophisticated systems have been proposed for accurate vehicle localization. However, most of the systems are aiming at autonomous driving and use high-cost devices such as stereo cameras, Velodyne, and even multiple sensors [8–12]. A low-cost device is preferred in the vehicle probe industry because it is easy to increase the number of equipped vehicles and enlarge the monitored area in urban areas. Currently, the commercial level GNSS receiver and Micro-Electro-Mechanical Systems (MEMS-level) accelerometer are available in driving data recorders and probe data collection devices. Thus, we focus on the improvement of the accuracy of probe vehicle data derived from the commercial level GNSS receiver and MEMS-level accelerometer sensor.

The Global Positioning System (GPS) was developed in the United States of America. GPS is the representative of GNSSs. After the GPS was introduced for public use, its data became one of the significant data sources for traffic analysis [13]. The GPS data were first used for traffic engineering in 1995 [14]. At that time, the experiments already demonstrated that the accuracy of GPS data is degraded in the central business district (CBD) of a city. Researchers addressed some of the

* Corresponding author.
E-mail address: guyanlei@kmj.iis.u-tokyo.ac.jp (Y. Gu).
Peer review under responsibility of International Association of Traffic and Safety Sciences.

https://doi.org/10.1016/j.iatssr.2018.03.001

key issues of a traffic monitoring system based on GPS-based probe vehicle reports (position, speed, or travel times) and concluded that they constitute a feasible source of traffic data [15]. However, the main drawback of GPS-based traffic analysis technology is that its low population penetration is not sufficient to provide an exhaustive coverage of the transportation network. Currently, with the popularization of onboard navigators or smartphones, the coverage rate has improved dramatically. Real-time traffic monitoring and broadcasting systems have been developed based on the GPS enabled smartphones. The results suggest that a 2%–3% penetration of cell phones of the driver population is enough to provide accurate measurements of the traffic flow velocity [16]. An increased number of studies used GPS-based probe data to analyze traffic situations; for example, GPS positioning results were utilized to measure the travel time [17,18]. The GPS-based probe data was used to evaluate the travel time variability [19]. The proposed ideas are quite successful with respect to road-network or link-level traffic monitoring. Because the link length is ~100 m in the city, the 15 m error of GPS data is not the most urgent issue of real-time traffic surveillance [20]. However, considering the significance of lane-level traffic analysis and the width of the vehicle lane (~3.5 m), reducing the GPS positioning error is necessary to improve the quality of probe data.

The GNSS receivers installed in commercial devices are usually low-cost, single-frequency, stand-alone modules. In open fields, this type of GNSS receiver achieves a satisfactory positioning performance [21]. However, it suffers from multipath and Non-Line-Of-Sight (NLOS) propagation caused by surrounding skyscrapers in urban canyons. In fact, the two effects, NLOS and multipath often occur together in urban canyons but they are not the same. In the case of NLOS, the signal is only received via reflection, no direct Line-of-Sight (LOS) path exists. Multipath means that the direct and reflected paths are received together. Therefore, they lead to pseudorange errors, resulting in positioning errors. These positioning errors could reach up to 100 m [22,23]. The huge positioning error challenges the lane-level requirements for probe data acquisition.

Many sophisticated algorithms using omnidirectional infrared cameras [24], shadow matching [25], or the Three-Dimensional (3D) Building Model [26] were developed to mitigate the multipath and NLOS effects. These methods were used to exclude unhealthy signals and mitigate the NLOS and multipath effects. However, the exclusion of satellites causes the distortion of the Horizontal Dilution of Precision (HDOP). To mitigate the NLOS and multipath effects while reducing the HDOP distortion, the 3D building map and ray-tracing technique were used to detect the NLOS and multipath effects and rectify the positioning result of the commercial GNSS single-frequency receiver [27–29]. The acronym of this technique is 3D-GNSS. Previous evaluations demonstrated that 3D-GNSS achieves a high performance in urban canyon environments [27–29] and significantly contributes to the localization system for autonomous driving [30–32]. Based on the effectiveness of the 3D-GNSS positioning method, we propose to acquire precise probe vehicle data utilizing this method.

The accelerometer has been adopted for the detection of different driving events (e.g., break, lane change, etc.) and to classify if these events are aggressive or not [33]. In addition, the accelerometer and gyroscope in smartphones are also used to classify different driving styles into three levels: normal, aggressive, and very aggressive [34]. Moreover, the accelerometer and GPS sensor were used as means to monitor road and traffic conditions [35,36]; potholes, bumps, and vehicle braking and honking can be detected. These studies proved the effectiveness of the accelerometer in driving event detection. In addition, vision based lane-change and lane-keep detection technology could be used to improve the correct lane rate and positioning accuracy [27–29]. In this paper, we propose to use an onboard accelerometer to detect lane-change and lane-keep events. Lane-change and lane-keep events can be used to rectify the positioning error of GNSS positioning results by referring to the 2D map including lane information.

Thus, three contributions are described in this paper. The first contribution is to employ the 3D-DGNSS positioning method for the acquisition the vehicle probe data and comprehensively evaluate the effectiveness of 3D-DGNSS-based probe technology. The evaluation includes both the position and speed domains. The second one is to develop a stop vehicle detection algorithm. The detection of the stop vehicle could be used to recognize the congestion situation in each vehicle lane. The third contribution is to adopt the accelerometer sensor to improve the correct lane rate of the positioning results estimated with the standalone GNSS technique. These three contributions are described in Sections 2 and 3. The experimental results are demonstrated in Section 5. Finally, discussion and conclusions are provided in Section 5.

2. Three-dimensional map-aided differential GNSS

In the urban environment, multipath and NLOS effects are the main reasons for the pseudorange measurement error. In addition, the ionospheric delay, tropospheric delay, satellite clock error, and system time differences of multiple GNSSs lead to positioning errors. We propose to eliminate the pseudorange error by using differential correction information and the 3D building model.

2.1. Differential GNSS correction

The 3D-DGNSS schematic is shown in Fig. 2. A reference station was installed for GNSS measurement. The position of the reference station was fixed and previously surveyed using precise point positioning (PPP) or other approaches. After differential correction, the correction was transmitted to the rover. The rover then employed it to common satellites to improve its own positioning accuracy.

For one satellite system, for example, the correction of the Differential Global Positioning System (DGPS) can be generated by calculating

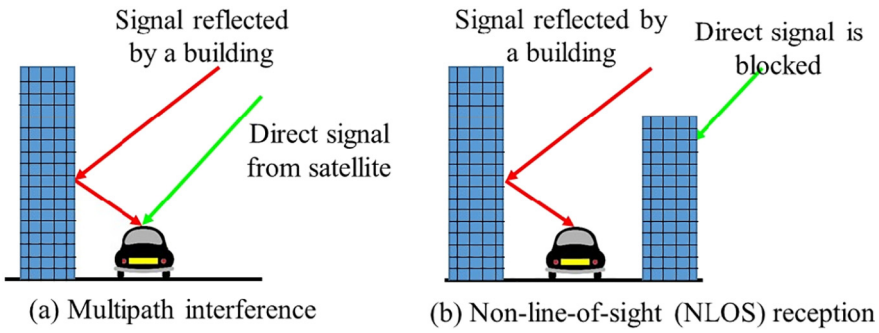

Fig. 1. Visualization of the multipath (a) and NLOS (b) effects [30].

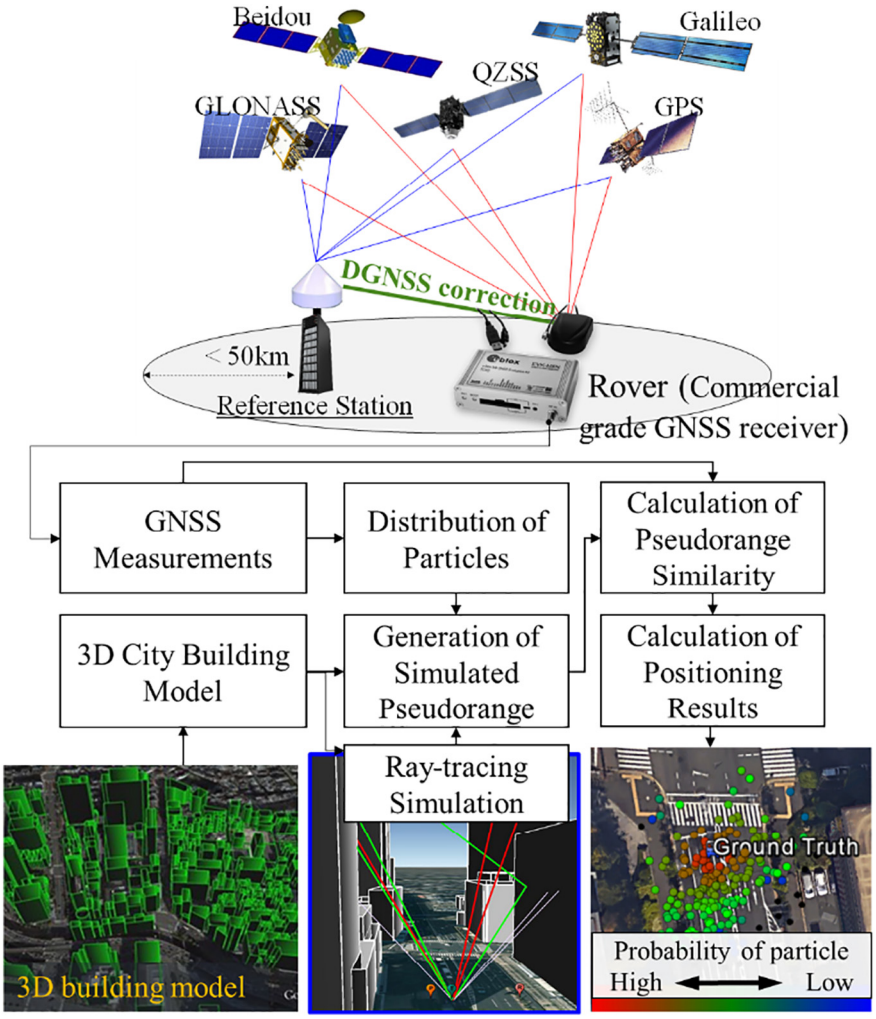

Fig. 2. Flowchart of GNSS positioning with the aid of differential correction and the 3D building model.

the difference between the true range and raw pseudorange for one satellite, as shown in Eq. (1):

$$\rho_{GPS}^{Corr} = \rho_{GPS}^{Ref} - \left(R^{Ref} + c\left(\Delta t_{RCV}^{Ref} - \Delta t^{SV}\right)\right) = I^{Ref} + T^{Ref} + MP^{Ref} + \varepsilon^{Ref}, \quad (1)$$

where ρ_{GPS}^{Corr} is the differential correction in the pseudorange domain of the GPS measurement, ρ_{GPS}^{Ref} denotes the GPS measurement received by the reference station, R^{Ref} is the true range between the reference station and satellite, Δt_{RCV}^{Ref} denotes the receiver clock bias compared with the GPS system time, Δt^{SV} is the satellite clock bias, and ε^{Ref} denotes the receiver thermal noise. The parameters I^{Ref} and T^{Ref} denote the ionospheric and tropospheric delays, respectively, and MP^{Ref} reflects the multipath and NLOS effects on the reference station. Theoretically, if the distance between the reference and rover station is below 50 km, the ionospheric delay, tropospheric delay, satellite clock error, and satellite orbit error of the rover station can be eliminated by applying differential correction. The positioning error of the rover station is therefore mainly caused by the multipath and NLOS effects. The GNSS includes not only the United States' GPS but also the European Galileo, Russian Global Navigation Satellite System (GLONASS), and Chinese Beidou Satellite Navigation and Positioning system. In the case of the multi-GNSS constellation, the system time offset between the GPS and other constellations can also be estimated with the DGNSS technique.

For example, the DGNSS correction of a GLONASS pseudorange measurement can be calculated using Eq. (2):

$$\rho_{GLONASS}^{Corr} = \rho_{GLONASS}^{Ref} - \left(R^{Ref} + c\left(\Delta t_{RCV}^{Ref} - \Delta t^{SV}\right)\right)$$

$$= c(\Delta t_{GPS-GLONASS}) + I^{Ref} + T^{Ref} + MP^{Ref} + \varepsilon^{Ref}, \quad (2)$$

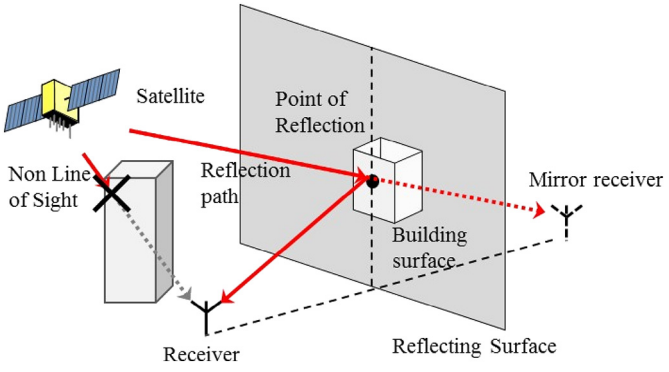

Fig. 3. Ray-tracing technique used in this research.

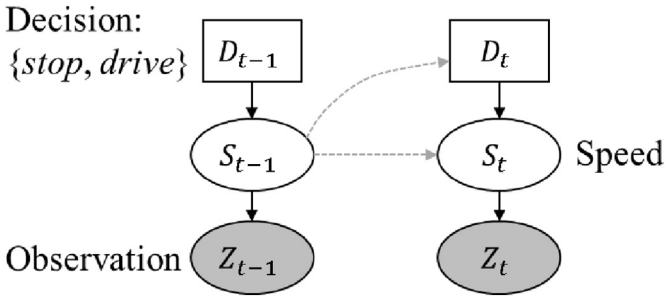

Fig. 4. Proposed dynamic bayesian network model for stop detection.

where $\Delta t_{GPS-GLONASS}$ denotes the system-time offset between the GLONASS and GPS. The satellite system time difference values of both the reference and rover station are the same. Therefore, the system time differences are eliminated. Differential positioning is therefore used to easily correct the system time difference when combining multiple satellite systems.

2.2. 3D Map-aided GNSS positioning with differential correction

After differential correction, the positioning error of the rover station is mainly caused by multipath and NLOS effects. To analyze and correct the pseudorange measurement error caused by multipath and NLOS, a 3D building map (3D Map) is needed. Two sets of map data are required for the establishment of the 3D map. The first set includes 2-dimensional building footprint data, named Fundamental Geospatial Data (FGD). The FGD is obtained from the Japan Geospatial Information Authority. The other one contains Digital Surface Model (DSM) data. The DSM data is provided by a Japanese company called Aero Asahi Corporation. The DSM data is used to obtain the height information of the building outline. Firstly, the coordinates of all corners of the building outline are sequentially extracted from the FGD. Subsequently, the height information of each determined corner is derived from the DSM data and attached to the corresponding corner. This way, the 3D map is generated. However, the 2-dimensional building outline data include an error of 1 to 2 m. We employed the map correction method proposed in previous work [37] to optimize the 3D building map of the experiment area in this research.

The first step of the 3D-DGNSS positioning method is to generate positioning candidates. The commercial GNSS receiver provides the "raw" user position. Moreover, to reduce the effect of the error of the "raw" user position, the predicted position is adopted as the other center of the candidate distribution. In this research, half of the Gaussian random candidates are generated based on the "raw" user position provided by the GNSS receiver and the other half are based on the predicted user position.

Secondly, after the distribution of candidates, the pseudorange simulated from each candidate point is calculated by ray tracing, as shown in Fig. 3. The calculation of the simulated pseudorange is based on following equations:

$$\hat{\rho}_n^{(i)} = R_n^{(i)} + c\left(\delta t^{r(i)} - \delta t_n^{sv}\right) + I_n + T_n + \varepsilon_n^{refl(i)} \tag{3}$$

$$\hat{\rho}_n^{(i)} = R_n^{(i)} + c\left(\Delta t_{RCV}^{Rover}\right) + \rho_n^{Corr} + \varepsilon_n^{refl(i)}, \tag{4}$$

where $R_n^{(i)}$denotes the geometric distance between the satellite n and simulated sample i; $c\delta t^{r(i)}$ is the receiver clock offset equivalent distance; $c\delta t_n^{sv}$ is the satellite clock offset equivalent distance; I_n is the ionospheric delay; T_n is the tropospheric delay; and $\varepsilon_n^{refl(i)}$ denotes the reflection delay distance estimated by the ray-tracing method. In fact, Eq. (3) can be represented as Eq. (4). The Δt_{RCV}^{Rover} parameter denotes the rover receiver clock bias compared with the GPS system time. It is optimized to minimize the difference between the simulated and measured sets. The parameter ρ_n^{Corr} is the differential correction information. Eqs. (1) and (2) explain the ρ_n^{Corr} based on the type of the satellite n.

One problem is the estimation of $\varepsilon_n^{refl(i)}$. The reflection delay $\varepsilon_n^{refl(i)}$ can be divided into three parts: LOS, multipath, and NLOS. The LOS signal is not affected by the buildings. Therefore, the reflection delay distance $\varepsilon_n^{refl(i)}$ is zero. In the case of the NLOS (Fig. 2), the calculation of the reflection delay is straightforward, that is, signal reflection path minus NLOS path. However, the multipath effect on the pseudorange is more ambiguous. This research assumes that the multipath effect is ~6 dB weaker than the LOS signal and the commercial receiver applies the strobe correlator [38] with a 0.2 chip spacing based on experience. These principles are used to simulate the pseudorange delay caused by the multiple path. In this step, both the reflection delay distance and satellite conditions are obtained.

Thirdly, to provide the accurate pseudorange similarity, we verify the condition of every satellite based on the signal strength. Basically, the C/N0 of the LOS signal should be higher than that of the NLOS signal. The multiple path case should be between NLOS and LOS. If the satellite condition determined by checking the C/N0 signal differs from that from ray tracing, the satellite is excluded and becomes invalid for the positioning calculation process.

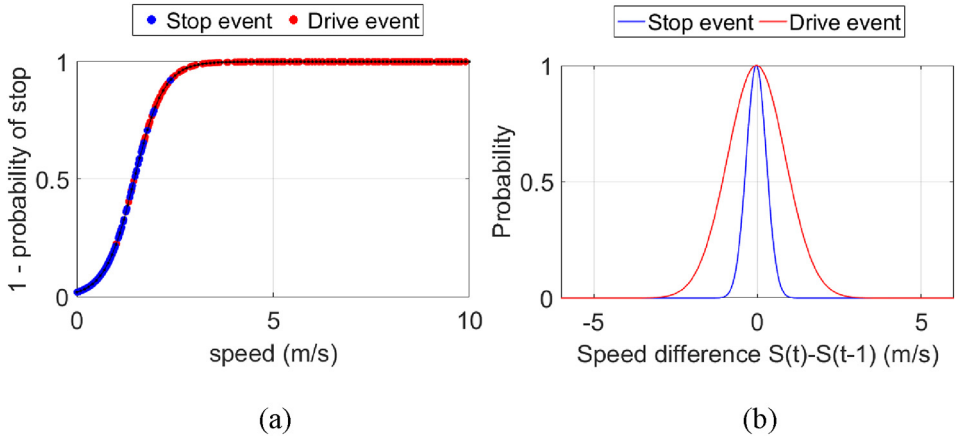

Fig. 5. Visualization of the learned parameters of the DBN model of stop detection.

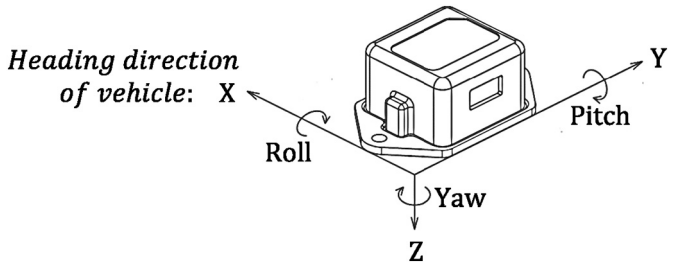

Fig. 6. Definition of accelerometer direction.

Fourthly, the likelihood of the candidate is calculated based on the similarity between the simulated and measured pseudoranges. It is defined by the following function:

$$\alpha^{(i)}(t) = \begin{cases} \exp\left[-\dfrac{D_{Pr}^{(i)2}}{\sigma_0^2}\right] & \left(\text{if } D_{pr}^{(i)} \mathbf{b} C_{\text{pr}}\right) \sim \text{valid} \\ \mathbf{0} & (\text{otherwise}) \sim \text{invalid} \end{cases}, \tag{5}$$

where $\alpha^{(i)}(t)$ denotes the likelihood function of the i-th candidate for the epoch t, $D_{Pr}^{(i)}$ is the averaged difference between the measured and simulated pseudoranges for all valid satellites, and σ_0 is the variance of $D_{Pr}^{(i)}$. This paper tunes the variance empirically; it is set to 20 m^2. To exclude the outlier candidate, this study defines a constant threshold, C_{pr}. The value of C_{pr} is adjusted to 10 m. The right picture in the bottom of Fig. 1 shows the invalid candidates and the valid candidates. The invalid candidates are marked black, and the valid candidates are marked with different colors to denote different likelihood values. Finally, the weighted average of the positions of all valid samples is the final rectified position, as shown in the equation below:

$$\mathbf{x}(t) = \frac{\sum_i \alpha^{(i)}(t)\, \mathbf{P}^{(i)}(t)}{\sum_i \alpha^{(i)}(t)}, \tag{6}$$

where $\mathbf{x}(t)$ is the position rectified by the proposed method and $\mathbf{P}^{(i)}$ is the position of the i-th candidate. Overall, this method uses the pseudorange similarity of the candidate to denote the confidence of the candidate for the final positioning.

3. Acquisition of precise probe vehicle data

In the acquisition of probe vehicle data, the vehicle position is estimated with the 3D-DGNSS method. The vehicle speed is directly calculated from the positioning results of two consecutive epochs. Based on the position and speed information, the stop detection and lane-level localization are developed.

3.1. Stop detection using the speed estimated from the 3D-DGNSS

In addition to vehicle speed and position, the discrete description of the vehicle state (stop or not) is significant for traffic analysis. Theoretically, if the GNSS positioning result is accurate enough, the stop state can be derived directly from the result. Generally, it is difficult to choose a constant threshold to distinguish the stop from the drive event based on the noise of the GNSS positioning results. The probabilistic estimation method is more robust for stop detection. The Dynamic Bayesian Network (DBN) has been widely used for sequential data analysis such as the analysis of various behaviors [39,40]. This paper also proposes to use the DBN model to recognize if the vehicle stops or not. The particle filter is adopted as inference technique. The proposed DBN model is shown in Fig. 4.

The square D_t reflects the decision about the stop at time t. It is connected to the node S_{t-1}, the estimated speed at time t-1. This means that the speed of the previous epoch affects the probability of the stop. In addition, node S_t is connected to the decision node D_t and speed node S_{t-1}. This design can explain the relationship of the speed change of different events. For example, in the drive case, the speed may change because of acceleration or deceleration, but the speed should not change in the stop case. Moreover, the speed node S_t is connected to the gray ellipse Z_t. Z_t is the observation node. This connection represents how similar the estimated speed is compared with the observed speed. The weight of each particle is estimated based on this connection. According to the proposed DBN mode, the probability of a stop for each particle can be formulated as:

$$P(D_t, S_t|S_{t-1}) = P(D_t|S_{t-1})P(S_t|S_{t-1}, D_t) \tag{7}$$

$$P(D_t|S_{t-1}) = \frac{1}{1 + \exp(-(\alpha + \beta S_{t-1}))} \tag{8}$$

$$P(S_t|S_{t-1}, D_t) \propto \exp\left(-\frac{((S_t - S_{t-1}) - \mu_{D_t})^2}{2\sigma_{D_t}^2}\right), \tag{9}$$

where, $P(D_t|S_{t-1})$ is a logistic function and α and β are the learned parameters. Eq. (8) explains the relationship between the speed and

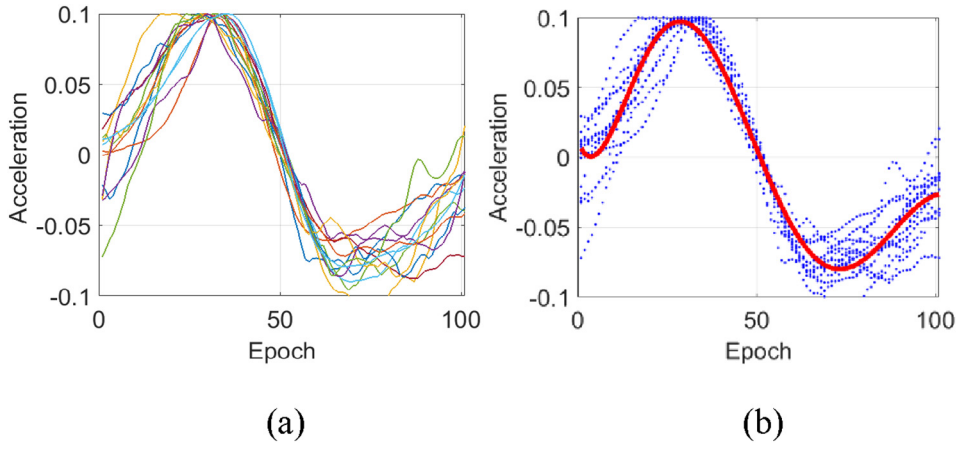

Fig. 7. (a) Centralized and normalized Y direction acceleration of multiple lane-change events, (b) Curve fitting using the acceleration of multiple lane-change events. The red curve is the learned template.

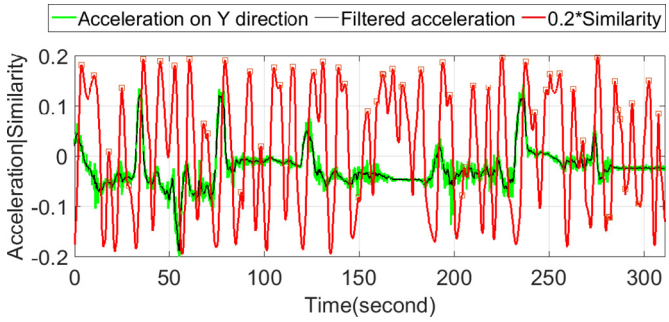

Fig. 8. Matching result for test data using the correlation and learned template.

stop event. Fig. 5a visualizes the two parameters using the training data. The red and blue points correspond to the drive events and stop data, respectively; the curve represents the learned model described in Eq. (8). We can see that the lower speed data have a higher stop probability and higher speed data indicate a lower stop probability. In other words, the learned model recognizes the stop and drive well using speed information.

The function $P(S_t|S_{t-1}, D_t)$ is the context Gaussian function. The context Gaussian function has different parameters for stop and drive contexts. The explanatory variable of the Gaussian function is $S_t - S_{t-1}$, that is, the speed change from the last to the current epoch. The parameters μ_{D_t} and σ_{D_t} represent the distribution of the speed change. These two parameters μ_{D_t} and σ_{D_t} are learned based on training data. Fig. 5b shows the two parameters. The blue curve has a narrower distribution compared with the red one. This narrower distribution means that the speed change in the stop context is relatively small. The speed change is caused by both the positioning error and vehicle acceleration in the drive case, but it is only caused by the positioning error in the stop case. In addition, the blue curve does not only concentrate on the position of zero because GNSS-based positioning results could not be fixed to a constant position, even if the vehicle stops because of the positioning error.

This paper adopts the particle filter as inference. The probability of each particle is estimated based on Eqs. (7) to (9). The probability of the stop decision at time t can be formulated as:

$$P(D_t) = \sum_{i=1}^{n} W_t^i P\left(D_t^i, S_t^i | S_{t-1}^i\right) \tag{10}$$

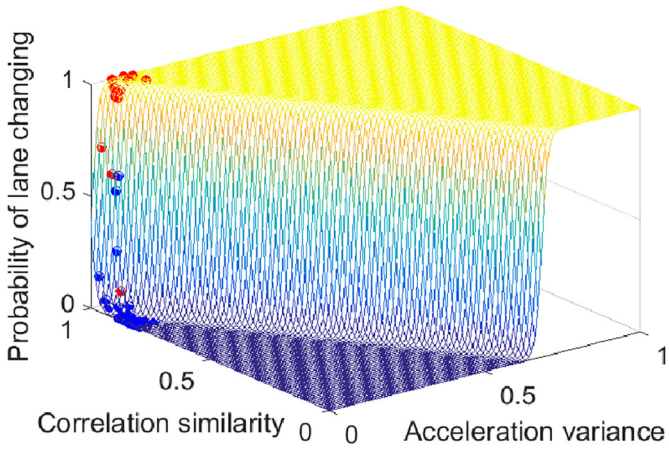

Fig. 9. Logistic regression for lane-change detection. The blue points are the non-lane-change data, red points are the lane-change data, and the curving surface illustrates the logistic regression result.

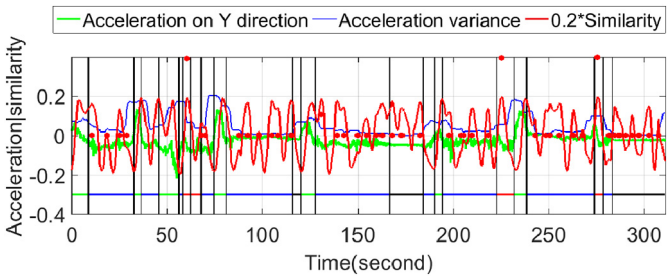

Fig. 10. Lane-change detection. The green curve is the Y direction acceleration, the red curve is the correlation result with a 0.2 scaling factor for clarity, and the blue curve is the variance of the acceleration in a time window. The lines at −0.3 indicate the ground truth of the type of behavior (blue: lane-keep, black: stop, green: turning, red: lane-change) and the red points denote the lane-change probability.

$$W_t^i = \exp\left(-\frac{\left(S_t^i - Z_t\right)^2}{2\sigma^2}\right), \tag{11}$$

where W_t^i is the weight of each particle, i is the index of the particles, Z_t is the speed calculated from the GNSS positioning result at time t, and σ is empirically set to 1 m/s in this research. The Eq. (11) means that the more similar the estimated speed S_t^i and the observed speed Z_t are, the higher the particle weight is.

3.2. GNSS lane-level localization with 3D-DGNSS and accelerometer

Our previous work indicated that lane-change and lane-keep events can be used to rectify the positioning error of the GNSS positioning results by referring to the 2D map with lane information [22,23]. This paper proposes to detect lane-change and lane-keep events using an accelerometer. The accelerometer is installed on the bottom of the vehicle; the direction of the accelerometer is illustrated in Fig. 6. The x-axis corresponds to the heading direction of the vehicle. The y-axis is the right side of the vehicle. In this research, we focus on the acceleration value along the y-axis because it can indicate the lane-change behavior. Generally, there are three events in drive: turning, lane-change, and lane-keep. The turning usually occurs at intersections or in road areas with curvature. Thus, these areas can be specified in the road map. The lane-change detection is performed when the GNSS positioning results are outside of these areas.

Template matching is used to distinguish the lane-change from lane-keep behavior. In this research, we use the right-direction lane-change as the example to explain the method. Firstly, multiple samples of lane-change events are collected. The collected samples are centralized and normalized in time direction (horizontal axis) such that the samples have the same time scale. Subsequently, the samples are normalized in acceleration direction (vertical axis). The centralized and normalized samples are shown in Fig. 7a. Each colored curve denotes one lane-change event. The centralization and normalizations can

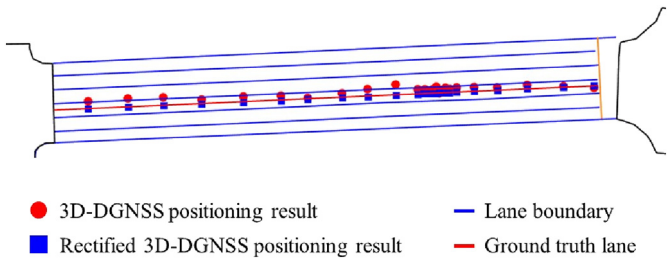

Fig. 11. Rectification for GNSS positioning results using the road map in the lane-keep case.

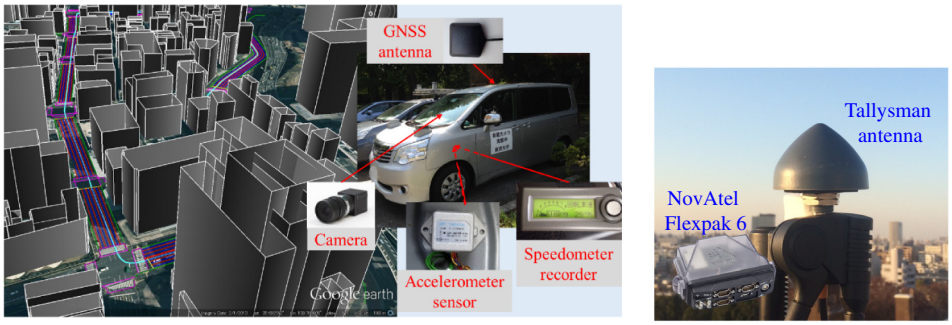

Fig. 12. (a) 3D building map, 2D lane-level road map, and experimental devices used in this research [31], (b) Antennas used at the reference station.

amplify the pattern. The curve-fitting method is then used to determine the acceleration pattern during a lane-change event, as shown in Fig. 7b.

After the template is obtained, the sliding window method is used for matching. Firstly, the data within a time window are extracted. The extracted data are then normalized in the horizontal and vertical directions, respectively. This data are called test data. Subsequently, the correlation coefficient between the test data and learned template is estimated to detect the candidates for lane-change events. The correlation can be described as follows:

$$C(T,L)=\frac{1}{N}\sum_{i=1}^{N}\left(\frac{T_i-\mu_T}{\sigma_T}\right)\left(\frac{L_i-\mu_L}{\sigma_L}\right), \tag{12}$$

where μ_T and σ_T are the mean and standard deviation of the test data, respectively; μ_L and σ_L are the mean and standard deviation of the learned template, respectively; N is the length of the data; and T_i and L_i are the i-th points of the test and template data, respectively. Fig. 8 visualizes the correlation result for example data with a length of 5 min. The green curve illustrates the change of the Y direction acceleration during drive. The correlation result is indicated by the red curve. The correlation result is scaled by a factor of 0.2 for clarity. There are several ten peaks. Each peak indicates that the pattern is similar to that of the learned template of the lane-change event. Solely using the similarity estimated based on the correlation is not enough to accurately recognize the lane-change event because there are many detected peaks.

To detect the lane-change events correctly, we propose to use one more feature: the acceleration variance in a local time window. The acceleration variance can be described as follows:

$$V_t = \max A - \min A \, A\in\{A_{t-k}, A_{t+k}\}, \tag{13}$$

where max$A$ is the maximum acceleration in the time window $\{t-k, t+k\}$ and min$A$ is the minimum acceleration. Thus, the similarity estimated by the correlation and acceleration variance are used together to recognize lane-change events from the candidates provided by only using the correlation.

To identify the relationship between the acceleration variance, correlation similarity, and probability of lane-change, we selected approximately 100 training data. The training data includes both lane-change and other events. Because this step only focuses on the candidates provided by the correlation step, we chose data with peaks in the template-matching process for the training. The two classes, that is, lane-change and non-lane-change, are expected to be separated by using the learned model. We propose to use logistic regression to identify the relationship. The model can be described as follows:

$$P((laneChange|\{A_{t-k}, A_{t+k}\})) = \frac{1}{1+\exp(-(\alpha+\beta_1 V_t+\beta_2 C_t))}, \tag{14}$$

where α, β_1 and β_2 are the learned parameters. C_t and V_t are the correlation similarity and acceleration variance defined by Eqs. (12) and (13), respectively. Fig. 9 shows the logistic regression result based on training data. The curving surface represents the learned model, the red points correspond to the lane-change, and blue points reflect non-lane-change data. Note that the learned model has the ability to recognize lane-change and non-lane-change. We use this model to decide if the candidate is lane-change or not.

Fig. 10 shows the lane-change detection result using pattern similarity and acceleration variance. Similar to Fig. 8, the correlation result is indicated by the red curve. The correlation result is scaled by a factor of 0.2 for clarity. There are several ten peaks. Subsequently, we applied the learned model (Fig. 9) to each peak to judge if the peak is lane-change or not. The red dots are the probability of lane-change for the peak candidates. This probability has been scaled by 0.3 for clarity. It is clear that most of the peaks have a low probability; only three peaks have a high probability (close to 1). These three peaks are in areas of lane-change events.

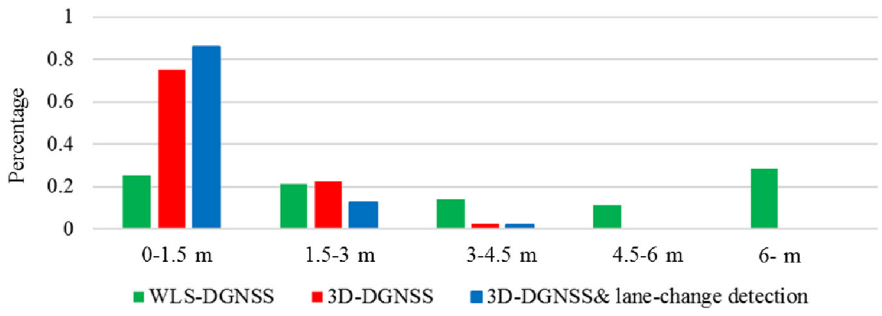

Fig. 13. Histogram of positioning errors in urban areas based on different methods.

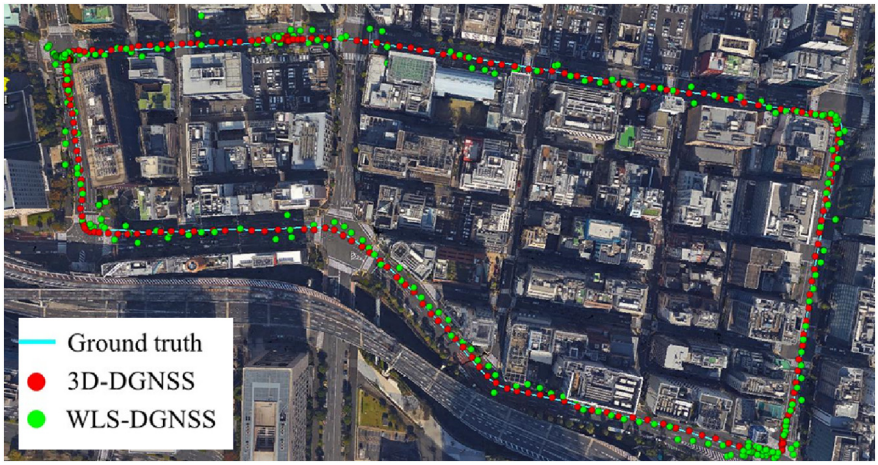

Fig. 14. Visualization of the positioning results of different GNSS positioning methods.

If there no lane-change behavior is detected in one road link, the GNSS positioning results will be rectified by determining the minimum distance from the GNSS trajectory to each possible lane center. The lane center information is included in the road map. Fig. 11 shows the rectification of the GNSS positioning results in a lane-keep case. The red points are the positioning results provided by the 3D-DGNSS method. The red line is the lane in which the vehicle was driven. The blue squares are the rectified positioning results. Because most of the red points are in the correct lane and the accelerometer also indicates that there is no lane-change event, we could rectify several red points in the neighboring lane to the correct lane. When lane-change is detected, this rectification method also can be used to improve the correct lane rate.

4. Experiment

4.1. Experiment setup

To evaluate the proposed 3D-DGNSS, we conducted experiments in the Hitotsubashi area of Tokyo. We chose this location for experiments because of the tall-building density. Fig. 12 shows the developed 3D building map, 2D lane-level road map, and experimental devices used in this research. In the experiment, a u-blox EVK-M8 GNSS model, a commercial level receiver, was used for the rover. It can receive signals from multiple GNSSs (GPS, GLONASS, and QZSS). We placed the u-blox receiver on top of our vehicle to conduct pseudorange measurements. In addition, we installed the reference station on the roof of our research building. The building is the highest building in the area. The distance from the reference station to the experiment area is less than 20 km. The output rate of both receivers is 1 Hz. In addition to the GNSS receiver, an accelerometer and speedometer were installed in the vehicle to measure the vehicle acceleration and velocity. Moreover, an onboard camera was installed in the vehicle. The camera captured the front-view images for the generation of the ground truth. The data from these sensors were synchronized in the experiments.

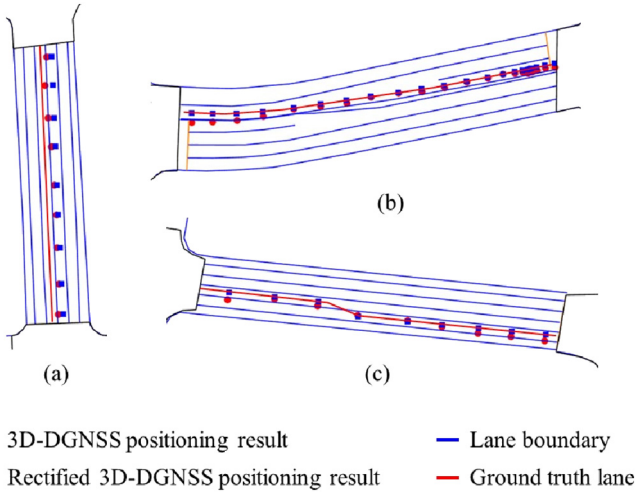

Fig. 15. Three cases of rectification of GNSS positioning results using a road map and lane-change detection.

The driving distance of each test is approximately 1500 m. We conducted multiple tests. During the vehicle self-localization, it is more important to distinguish which lane the vehicle is in compared with the positioning accuracy. Therefore, we evaluated the performance of the localization system based on both the lateral error and correct lane rate. We manually distinguished the ground truth trajectory of our vehicle by referring to the image from the onboard camera and a high-resolution aerial image. In this paper, we only evaluated the lateral error from the positioning points to the true path because it is very difficult to determine the true longitudinal position of the vehicle in the link when the vehicle moves. In addition, for lane-level traffic analysis, the lateral position error could represent how correct the localization of the car in the true lane is. Moreover, the ground truth of stop, drive, lane-change, and lane-keep events was obtained from the image from the onboard camera. For stop detection, we observed the image from the onboard camera and decided if the car stopped or not. We manually determined the ground truth every second. The ground truth of the speed was obtained every second from vehicle speedometer data. We also optimized the speed value in the low-speed situation using the image from the onboard camera.

4.2. Evaluation for localization accuracy

To understand the benefit of the proposed 3D-DGNSS in urban canyon environments, this paper compares the 3D-DGNSS with the widely used Weighted Least Square based Differential GNSS (WLS-DGNSS). Different aspects of the results are compared including the positioning error, availability, and correct lane rate. The availability denotes how many of 100 epochs provide results. The correct lane rate indicates the percentage of the localization results that agrees with the lane in which we drove in the experiment. For example, we drove 100 s in the third lane of a road in the experiment, and the localization results have 80 epochs (1 epoch/s) in the third lane. In this case, the correct lane rate is 80%. As indicated in Table 1, the developed 3D-DGNSS has a mean positioning error of 1.09 m and a correct lane rate of 74.8% in the urban area. However, the conventional method WLS-DGNSS has a

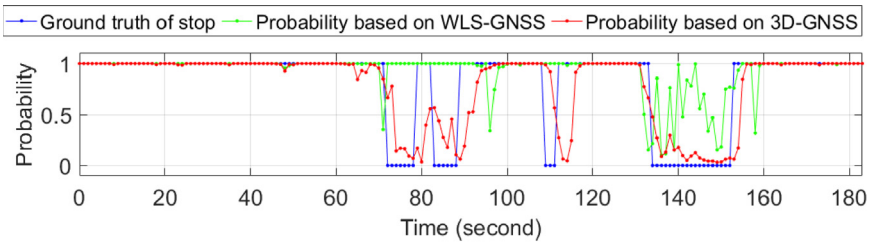

(a) Stop detection based on different GNSS positioning methods

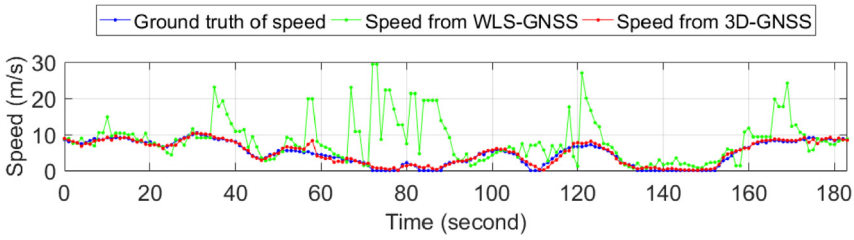

(b) Speed estimation based on different GNSS positioning methods

Fig. 16. Stop detection using the speed calculated from different GNSS positioning methods.

mean positioning error of 4.72 m and only achieves a correct lane rate of 23.8%. Fig. 13 shows the histogram of the positioning errors of different methods. The horizontal axis of the histogram is the range of the positioning error. The interval of the horizontal axis is set to 1.5 m. 1.5 m is approximately the half-width of a vehicle lane. The vertical axis means how much percentage of positioning results have the corresponding error. About 50% of WLS-DGNSS positioning results (green bars) have the error more than 3 m. In contrast, 3D-DGNSS positioning method (red bars) and integration with lane-change detection (blue bars) have better performance. About 70% of 3D-DGNSS positioning results have the error less than 1.5 m. In addition, integration of 3D-DGNSS and lane-change detection provides more accurate results compared to 3D-DGNSS only. To understand the magnitude of improvement based on the usage of the 3D-DGNSS, the experimental results of one test are visualized using Google Earth (Fig. 14). The 3D-DGNSS and WLS-DGNSS results are indicated by red and green dots, respectively. The cyan line is the ground truth. The positioning results of the 3D-DGNSS method are much more accurate than that of the WLS-DGNSS.

In this study, we propose to use an accelerometer to detect the lane-change event and improve the positioning error and correct lane rate of localization. In total, 75% of the lane-change events can be correctly recognized and lane-keep events were not incorrectly detected. Fig. 15 shows the results of the positioning rectification method for three cases. Cases a and b are the lane-keep events. Because most of the GNSS positioning results are in the correct lane, the rectification can improve the correct lane rate of localization in case b. However, the Fig. 15a shows a failed case. Note, however, that the number of this type of case is smaller than that of successful cases in all experiments. Thus, the total correct lane rate improved. In addition, the case c illustrates the rectification result for a lane-change event. Because of the successful detection of the lane-change using an accelerometer, the GNSS positioning results can also be rectified based on the lane-change moment. Finally, the correct lane rate could be improved to 87.1%. The positioning error was reduced to 0.51 m, as shown in Table 1. We can conclude that accelerometer-based lane-change detection can improve the stand-alone GNSS positioning method.

4.3. Evaluation of the speed error and stop detection

Fig. 16 demonstrates the speed estimation and stop detection results based on the WLS-DGNSS and 3D-DGNSS in one test, respectively. The green and red lines in Fig. 16a indicate the stop probability estimated with the WLS-DGNSS and 3D-DGNSS, respectively. The blue line is the ground truth for the stop case. The green and red lines in Fig. 16b are the speeds from the WLS-DGNSS and 3D-DGNSS, respectively. Note that the 3D-DGNSS-based stop detection performs better than the WLS-DGNSS-based stop detection. The main reason for that is that the WLS-DGNSS is not reliable and the 3D-DGNSS can provide a more accurate speed. For example, the WLS-DGNSS speed and stop recognition result in the first stop area (around epoch 90) is completely wrong. Although the speed calculation using the WLS-DGNSS in the fourth stop area becomes more accurate, the accuracy is still not sufficient to distinguish the stop from drive.

As shown in Table 2, the speed error of the 3D-DGNSS is smaller than 1 m/s. The 3D-DGNSS is much more accurate than the WLS-DGNSS-based speed estimation. In addition, a comparison of WLS-DGNSS and 3D-DGNSS stop detection was conducted. Table 3 shows the detection

Table 1
Comparison of different positioning methods in urban areas.

Positioning methods	Mean positioning error (m)	Standard deviation of the positioning error (m)	Availability	Correct lane rate
WLS-DGNSS	4.72	4.88	95.3%	23.8%
3D-DGNSS	1.09	0.86	96.8%	74.8%
3D-DGNSS and lane-change detection	0.51	0.82	96.8%	87.1%

Table 2
Comparison of the speed estimation in urban areas using different GNSS positioning methods.

Positioning methods	Speed error mean (m/s)	Speed standard error (m/s)
WLS-DGNSS	4.27	6.26
3D-DGNSS	0.90	0.92

Table 3
Detection rate of stop and drive using WLS-DGNSS and 3D-DGNSS.

WLS-DGNSS based stop detection		Real	
		Stop	Drive
Estimation	Stop	59.5%	3.4%
	Drive	40.5%	96.6%
3D-DGNSS-based stop detection		Real	
		Stop	Drive
Estimation	Stop	91.9%	5.9%
	Drive	8.1%	94.1%

rate based on the two methods. In fact, both the WLS-DGNSS and 3D-DGNSS perform well in drive detection. However, the 3D-DGNSS shows much better performance in stop detection. The reason for that is that the positioning results of the WLS-DGNSS scatter around the stop position and the speed from the scattered data shows a value similar to that of drive events. However, the 3D-DGNSS shows very low speed values during stop events. Therefore, the 3D-DGNSS shows a reliable and balanced performance in both stop and drive detection.

5. Conclusion and future work

This research proposes to use the 3D-DGNSS to generate precise probe vehicle data. The evaluations indicate that the developed 3D-DGNSS method has a positioning error of 1.09 m and a correct lane rate of 74.8% in the urban area. In addition, we propose to use the template-matching method to detect lane-change events in accelerometer data and further improve the position error and correct lane rate of GNSS positioning results. Finally, with the aid of lane-change detection, the correct lane rate can be improved to 87.1%. The positioning error was reduced to 0.51 m. These 3D-DGNSS-based positioning results are much better than that of the conventional GNSS method. Moreover, we extended the evaluation from positioning estimation to speed estimation. The 3D-DGNSS achieves a mean error of 0.9 m/s in the speed estimation. To directly reflect the advantage of accurate speed estimation for traffic situation analysis, we developed a probabilistic algorithm for stop detection. More than 90% of stops can be correctly recognized based on 3D-DGNSS results. Both the speed error and stop detection rate of the 3D-DGNSS are better than that of the conventional GNSS method.

One of the most important challenges in city development is to improve the utilization rate of vehicle lanes. A large amount of traffic data with accurate vehicle trajectories needs to be analyzed. More specifically, a good lane-level localization accuracy is required to conduct this type of analysis. The proposed method achieves a correct lane rate of 87.1%. Based on these accurate positioning results, lane utilization rate analysis could achieve more precise results. In addition to the lane utilization rate, the vehicle speed is another important parameter for traffic analysis. Because of the accurate positioning result of the 3D-DGNSS, the speed estimation has a small error of 0.9 m/s. This accurate speed can be used to determine if the traffic completely stopped or is slowly moving. By combining the positioning results and speed, the 3D-DGNSS can be used to analyze the traffic situation of each lane, for example, how many vehicles use this lane, what is the average speed of each lane, how often does congestion occur in each lane, and what is the difference between two neighboring lanes.

Acknowledgment

The authors acknowledge the Grant-in-Aid for Japan Society for the Promotion of Science (JSPS) (16F16350) Postdoctoral Fellowship for Oversea Researchers.

References

[1] M. Senbil, K. Ryuichi, The optimal duration for a travel survey: empirical observations, International Association of Traffic and Safety Sciences (IATSS) research, 33, 2, 2009, pp. 54–61.
[2] S. Kawasaki, The Challenges of Transportation/traffic Statistics in Japan and Directions for the Future, 39, 1, International Association of Traffic and Safety Sciences (IATSS) Research, 2015 1–8.
[3] L.B. Robert Qing, J.W.C. Van Lint, P.H. Serge, A theoretical framework for traffic speed estimation by fusing low-resolution probe vehicle data, IEEE Trans. Intell. Transp. Syst. 12 (3) (2011) 747–756.
[4] T. Seo, T. Kusakabe, Y. Asakura, Traffic state estimation with the advanced probe vehicles using data assimilation, Proceedings of 2015 18th IEEE International Conference on Intelligent Transportation Systems (ITSC) 2015, pp. 824–830.
[5] E. Jenelius, H.N. Koutsopoulos, Travel time estimation for urban road networks using low frequency probe vehicle data, Transp. Res. B Methodol. 53 (2013) 64–81.
[6] S.Y. Rompis, M. Cetin, F. Habtemichael, Probe vehicle lane identification for queue length estimation at intersections, J. Intell. Transp. Syst. 22 (2017) 10–25.
[7] J. Du, J.B. Matthew, Next-generation automated vehicle location systems: positioning at the lane level, IEEE Trans. Intell. Transp. Syst. 9 (1) (2008) 48–57.
[8] J. Choi, Hybrid map-based SLAM using a Velodyne laser scanner, Proceedings of 2014 17th IEEE International Conference on Intelligent Transportation Systems 2014, pp. 3082–3087.
[9] M. Schreiber, C. Knoppel, U. Franke, Laneloc: lane marking based localization using highly accurate maps, Proceedings of Intelligent Vehicles Symposium, 2013, 2013, pp. 449–454.
[10] H. Lategahn, C. Stiller, City GPS using stereo vision, Proceeding of 2012 IEEE International Conference on Vehicular Electronics and Safety (ICVES) 2012, pp. 1–6.
[11] J. Levinson, M. Michael Montemerlo, T. Sebastian, Map-based precision vehicle localization in urban environments, Robotics: Science and Systems, vol. 4, 2007, pp. 1–8.
[12] J. Zhang, S. Singh, LOAM: Lidar odometry and mapping in real-time, Proceedings of the Robotics: Science and Systems Conference (RSS) 2014, pp. 14–16.
[13] N. Uno, F. Kurauchi, H. Tamura, Y. Iida, Using bus probe data for analysis of travel time variability, J. Intell. Transp. Syst. 13 (1) (2009) 2–15.
[14] R. Zito, G. D'Este, M.A.P. Taylor, Global positioning systems in the time-domain-how useful a tool for intelligent vehicle-highway systems? Transp. Res. C 3 (4) (1995) 193–209.
[15] K. Sanwal, J. Walrand, Vehicles as probes, California PATH Working Paper, Institute of Transportation Studies, University of California, Berkeley, CA 1995, pp. 1–27.
[16] J.C. Herrera, D.B. Work, R. Herring, X.J. Ban, Q. Jacobson, A.M. Bayen, Evaluation of traffic data obtained via GPS-enabled mobile phones: the mobile century field experiment, Transp. Res. C 18 (4) (2010) 568–583.
[17] M. Tsuge, M. Tokunaga, K. Nakano, M. Sengoku, On estimation of link travel time in floating Car systems, Int. J. Intell. Transp. Syst. Res. 8 (3) (2010) 175–187.
[18] E. Jenelius, H.N. Koutsopoulos, Travel time estimation for urban road networks using low frequency probe vehicle data, Transp. Res. B Methodol. 53 (2013) 64–81.
[19] N. Uno, F. Kurauchi, H. Tamura, Y. Iida, Using bus probe data for analysis of travel time variability, J. Intell. Transp. Syst. 13 (1) (2009) 2–15.
[20] K. Liu, T. Yamamoto, T. Morikawa, Feasibility of using taxi dispatch system as probes for collecting traffic information, J. Intell. Transp. Syst. 13 (1) (2009) 16–27.
[21] S. Rezaei, R. Sengupta, Kalman filter-based integration of DGPS and vehicle sensors for localization, IEEE Trans. Control Syst. Technol. 15 (6) (2007) 1080–1088.
[22] Z. Wang, S. He, Y. Leung, Applying mobile phone data to travel behaviour research: A literature review, Travel Behaviour and Society, 2017.
[23] G. MacGougan, G. Lachapelle, R. Klukas, K. Siu, L. Garin, J. Shewfelt, G. Cox, Performance analysis of a stand-alone high-sensitivity receiver, GPS Solutions 6 (3) (Dec. 2002) 179–195.
[24] J.I. Meguro, T. Murata, J.I. Takiguchi, Y. Amano, T. Hashizume, GPS multipath mitigation for urban area using omnidirectional infrared camera, IEEE Trans. Intell. Transp. Syst. 10 (2009) 22–30.
[25] P.D. Groves, Shadow matching: a new GNSS positioning technique for urban canyons, J. Navig. 64 (3) (2011) 417–430.
[26] M. Obst, S. Bauer, P. Reisdorf, G. Wanielik, Multipath detection with 3D digital maps for robust multi-constellation GNSS/INS vehicle localization in urban areas, Proceedings of the IEEE Intelligent Vehicles Symposium 2012, Alcala de Henares, Spain 2012, pp. 184–190.
[27] L.-T. Hsu, Y. Gu, S. Kamijo, 3D building model based pedestrian positioning method using GPS/GLONASS/QZSS and its reliability calculation, GPS Solutions (2015) 1–16.
[28] L.-T. Hsu, Y. Gu, S. Kamijo, NLOS correction/exclusion for GNSS measurement using RAIM and city building models, Sensors 15 (7) (2015) 17329–17349.
[29] L.-T. Hsu, Y. Gu, S. Kamijo, Autonomous driving positioning using building model and DGNSS, Proceedings of Navigation Conference (ENC), 2016 European 2016, pp. 1–7.
[30] Y. Gu, L.T. Hsu, S. Kamijo, GNSS/on-board inertial sensor integration with the aid of 3D building map for lane-level vehicle self-localization in urban canyon, IEEE Trans. Veh. Technol. 65 (6) (2016) 4274–4287.
[31] Y. Gu, L.T. Hsu, S. Kamijo, Passive sensor integration for vehicle self-localization in urban traffic environment, Sensors 15 (12) (2015) 30199–30220.
[32] Y. Gu, L.T. Hsu, S. Kamijo, Vehicle localization based on three-dimensional map aided global navigation satellite system, Proceedings of Transportation Research Board 96th Annual Meeting (TRB), 2017.
[33] C. Saiprasert, T. Pholprasit, S. Thajchayapong, Detection of driving events using sensory data on smartphone, Int. J. Intell. Transp. Syst. Res. 15 (1) (2017) 17–28.

[34] D.A. Johnson, M.M. Trivedi, Driving style recognition using a smartphone as a sensor platform, Proceedings of 2011 14th International IEEE Conference on Intelligent Transportation Systems (ITSC) 2011, pp. 1609–1615.
[35] P. Mohan, V.N. Padmanabhan, R. Ramjee, Nericell: rich monitoring of road and traffic conditions using mobile smartphones, Proceedings of the 6th ACM Conference on Embedded Network Sensor Systems 2008, pp. 323–336.
[36] M. Fazeen, B. Gozick, R. Dantu, M. Bhukhiya, M.C. González, Safe driving using mobile phones, IEEE Transactions on Intelligent Transportation Systems, 13, 2012, pp. 1462–1468.
[37] Y. Gu, Y. Wada, L.-T. Hsu, S. Kamijo, SLAM with 3Dimensional-GNSS, Proceedings of IEEE/ION PLANS, 2016, 2016, pp. 190–197.
[38] M.S. Braasch, Performance comparison of multipath mitigating receiver architectures, Proc. In Proceedings of 2001 International IEEE Conference on Aerospace, vol. 3, 2001, pp. 1309–1315.
[39] Y. Hashimoto, Y. Gu, L.T. Hsu, M. Iryo-Asano, S. Kamijo, A probabilistic model of pedestrian crossing behavior at signalized intersections for connected vehicles, Transp. Res. C 71 (2016) 164–181.
[40] Y. Gu, Y. Hashimoto, T. Hsu, M. Iryo-Asano, S. Kamijo, Human-Like Motion Planning Model for Driving in Signalized Intersections, International Association of Traffic and Safety Sciences (IATSS) Research, 2016.